



Use of remote sensing-derived fPAR data in a grapevine simulation model for estimating vine biomass accumulation and yield variability at sub-field level

L. Leolini¹ · S. Bregaglio² · F. Ginaldi² · S. Costafreda-Aumedes^{1,3} · S. F. Di Gennaro³ · A. Matese³ · F. Maselli³ · G. Caruso⁴ · G. Palai⁴ · S. Bajocco² · M. Bindi¹ · M. Moriondo^{1,3}

Accepted: 10 October 2022 / Published online: 25 October 2022
© The Author(s) 2022

Abstract

Grapevine simulation models are mostly used to estimate plant development, growth and yield at plot scale. However, the spatial variability of pedologic and micro-climatic conditions can influence vine growth, leading to a sub-field heterogeneity in plant vigor and final yield that may be better estimated through the assimilation of high spatial resolution data in crop models. In this study, the spatial variability of grapevine intercepted radiation at fruit-set was used as input for a grapevine simulation model to estimate the variability in biomass accumulation and yield in two Tuscan vineyards (Sites A and B). In Site A, the model, forced with intercepted radiation data as derived from the leaf area index (LAI), measured at canopy level in three main vigor areas of the vineyard, provided a satisfactory simulation of the final pruning weight ($r^2=0.61$; RMSE = 19.86 dry matter g m⁻²). In Site B, Normalized Difference Vegetation Index (NDVI) from Sentinel-2A images was firstly re-scaled to account for canopy fraction cover over the study areas and then used as a proxy for grapevine intercepted radiation for each single pixel. These data were used to drive the grapevine simulation model accounting for spatial variability of plant vigor to reproduce yield variability at pixel scale ($r^2=0.47$; RMSE = 75.52 dry matter g m⁻²). This study represents the first step towards the realization of a decision tool supporting winegrowers in the selection of the most appropriate agronomic practices for reducing the vine vigor and yield variability at sub-field level.

Keywords Grapevine modeling · Normalized difference vegetation index · Precision viticulture · Sentinel-2A imagery · UAV imagery

✉ L. Leolini
luisa.leolini@unifi.it

Extended author information available on the last page of the article

Introduction

Grapevine (*Vitis vinifera* L.), with a global cultivated area of 7.3 million hectares, is one of the main components of agricultural systems worldwide (OIV, 2020). One third of this area is cultivated in Italy, France and Spain, which contribute almost 50% to the global wine production (OIV, 2020), so representing a key economic asset (Santos et al., 2020), and the typical cultural landscape of many agricultural regions (Barbera & Cullotta, 2016).

Since wine production and quality is largely affected by the spatial variability of pedo-environmental conditions, the adoption of precision agriculture techniques aimed at optimizing management improves uniformity of yields and product quality (Arnó et al., 2009; Brook et al., 2020; Matese et al., 2015). Indeed, the early detection of vine growth conditions and the advanced scheduling of farm practices (e.g. harvest) is crucial where the vine growing cycle is exposed to the impact of climate change (Biasi et al., 2019; Hannah et al., 2013; Leolini et al., 2018b; Moriondo et al., 2011, 2013; Wolkovich et al., 2018). In this context, process-based models are the preferred tools for assessing the effects of the environment on plant development and growth since they describe potential biomass accumulation as limited by nutrient or water stress (Bindi et al., 1997a, 1997b; Leolini et al., 2018a; Moriondo et al., 2007, 2019; Sinclair, 1986). However, crop growth models usually require many inputs to define local environmental conditions, such as weather, soil and management practices, and for monitoring the ongoing growing season, so limiting their application to the plot scale where this information is generally fully available. In a context of precision agriculture, the detailed real time description of field conditions is required for an optimized management of agronomic practices and farm scheduling. For this reason, process-based models which need large amounts of input data might not be a readily available approach for simulating the spatial variability of plant processes when the resolution scale is extended to farm or regional scale (Basso et al., 2001; Challinor et al., 2004).

The crop model reliability to robustly simulate plant growth processes may therefore be improved with information derived by remote sensing (RS) platforms, which provide data to force or update simulated state variables to observed values (e.g. derived from radiometric observations) (Clevers et al., 2002; Maselli et al., 2013; Moulin et al., 1998), with the purpose of increasing model accuracy at field level (Basso et al., 2001; Clevers et al., 1994; Ginaldi et al., 2019; Moriondo et al., 2007). Considering that plant canopy development and their light interception capability assume a relevant role in physiological processes such as transpiration and photosynthesis (Mabrouk et al., 1997; Mezghani et al., 2016), many efforts focused on deriving leaf area index (LAI) values or fPAR (fraction of the Photosynthetically Active Radiation) estimates from RS vegetation indices to feed crop models. Despite the approach being successfully adopted for sowing crops such as rice (Gilardelli et al., 2019; Setiyono et al., 2018), wheat (Guo et al., 2018; Moriondo et al., 2007), soybean (Basso et al., 2001) and maize (Fang et al., 2008, 2011), it has been still little applied on perennial crops with a few exceptions like olive tree (Leolini et al., 2022; Maselli et al., 2012) and jujube fruit tree (Bai et al., 2019). This is likely due to the inherent difficulty in disentangling the relative contribution of the various components of the agro-ecosystem to the vegetation index signal: the tree canopy and herbaceous layer (Maselli et al., 2012). These components may vary both during the season and within field depending on environmental conditions and management practices, so the assimilated normalized difference vegetation index (NDVI) signal must be partitioned among agro-ecosystem elements by the use of segmentation algorithm procedures (Cinat et al., 2019; Di Gennaro & Matese, 2020; Sozzi et al., 2020). Most of the available studies propose

multiple data assimilation at several stages during the season, thus increasing the number of external inputs required (e.g. RS images; Basso et al., 2001; Huang et al., 2015; Zhao et al., 2013). Although a larger amount of multi-temporal data can increase yield prediction accuracy, this procedure requires either specialized staff and several field campaigns (e.g. UAVs images, Ziliani et al., 2018), or time-consuming data post-processing and quality-checks (e.g. satellite images, Matese et al., 2015), with detrimental effects on the timing of estimation of vine yield. Indeed, despite it having been demonstrated that the simulation accuracy increases with a higher number of observations closer to the target event (Basso et al., 2001), an advanced prediction of actual field conditions can lead to useful information for farmers to identify the most appropriate management practices.

On this basis, this study intends to take steps forward in the integration between a grapevine growth model and satellite data, resolving the issue of accurately simulating vine biomass accumulation variability at sub-field level using a limited number of remotely sensed information. The aim of this work is to evaluate the feasibility of a forcing strategy based on remotely sensed canopy fPAR obtained at a single early stage (fruit-set) to guide the light interception in a crop simulation model (UNIFI.GrapeML, Leolini et al., 2018a, 2019). This methodology was tested in two Tuscan vineyards (Sangiovese variety) for estimating the variability of biomass accumulation at the end of the season, and then extended to a larger scale to perform a spatially explicit estimation of the plant growth processes, focusing on water balance and final yield as ground truth.

Materials and methods

Study area

The study was conducted in two vineyards where Sangiovese grapevine variety is grown (*Vitis vinifera* L.), located in Tuscany region, Italy:

- (1) The first vineyard (Site A, 0.5 ha, N–S oriented) is situated at Suvereto (Leghorn, 43° 04' 36.4" N 10° 41' 43.4" E; Fig. 1) and is characterized by a typical Mediterranean climate with hot-dry summers and mild winters (Koppen, 1936). Annual air temperature was 15 °C during the period 1950–2019, with the average maximum air temperature recorded in August (29 °C) and average minimum air temperature in January (3.1 °C; E-OBS dataset, www.ecad.eu). The annual average amount of precipitation (1950–2019) was 685 mm. The experiment was conducted in 2015, when average air temperature was 21.4 °C during the grapevine growing season (April–October) and precipitation was 198 mm. The soil texture is clay-loam (28% clay, 53% sand and 19% silt), tilled from budbreak to harvest to control weeds. The vines, planted in 1999, were trained with a Guyot system (5–7 shoots per plant) at a planting density of 2.4 m × 0.8 m. The vineyard follows the standard protocols of organic viticulture and agronomic practices such as composted sheep manure distribution, shoot positioning and pruning, and pest control with sexual confusion technique, copper and sulfur distribution (Caruso et al., 2017).
- (2) The second vineyard (Site B, 1.4 ha, NW–SE oriented) is located at Fonterutoli (Siena, 43° 25' 45.30" N, 11° 17' 17.92" E; Fig. 1) and is characterized by a Mediterranean climate (Koppen, 1936). Annual average air temperature was 13 °C during the period 1950–2019 with the average maximum air temperature recorded in August (28.6 °C)

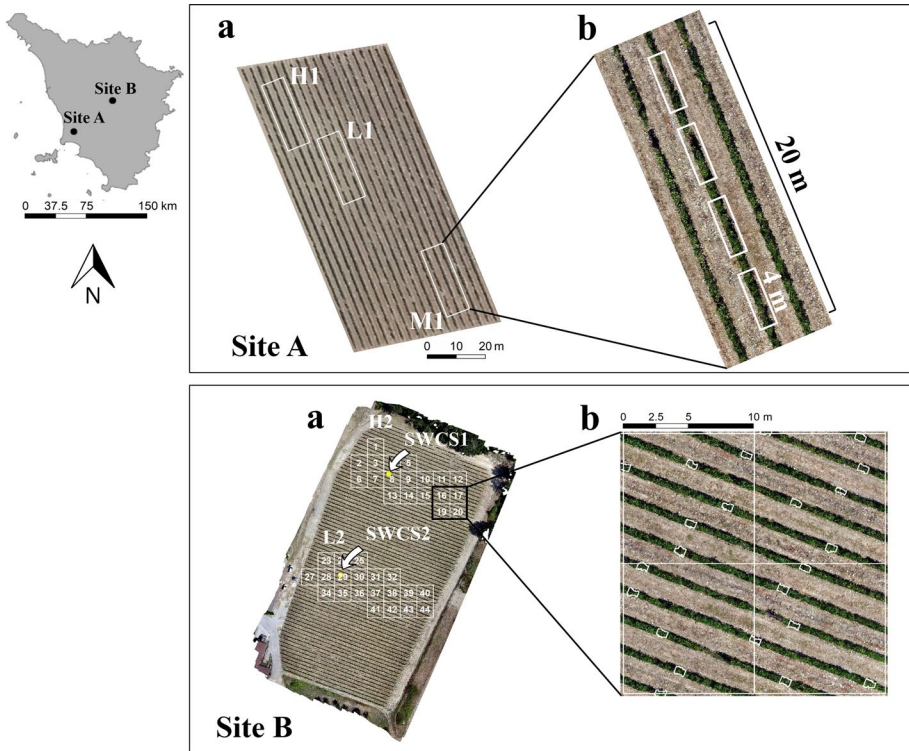


Fig. 1 Location and experimental design of the vineyard study cases (Site A and B) in Tuscany region. **a** Vineyard distribution of vigor areas, Site A: High (H1), Medium (M1) and Low (L1) vigor areas; Site B: High (H2) and Low (L2) vigor areas in Sentinel-2A grid (white squares). **b** Sampling scheme on the vineyard row: three adjacent rows of 20 m used for LAI measurements with four replicates of 4 m used for pruning weight data collection only in the central row (white squares; Site A), and white patches (Site B) used for vegetation and yield measurements. In Site B, Soil Water Content Sensors (SWCS1 and SWCS2) were positioned in the pixels 8 and 29 of H2 and L2 vigor zones, respectively

and average minimum air temperature recorded in January (1.1 °C; E-OBS dataset, www.ecad.eu). The average annual precipitation was 910 mm (1950–2019). The experiment was conducted in 2018, when the grapevine growing season had an average air temperature of 19.2 °C with a peak of 37.2 °C in July. The total amount of precipitation was 344 mm, concentrated in April–May and August–September (source <https://www.sir.toscana.it/>). The vineyard (slope 22%) is located in a hilly area where stable meadow, arable land, olive groves and vineyards are dominant, and soil texture is loam (23% clay, 34% sand and 43% silt; FAO/IIASA/ISRIC/ISSCAS/JRC, 2012). The vines were planted in 2008 and trained as a single cordon spur-pruned using a vertical shoot-positioned trellis (8 shoots per plant on average) at a planting density of 2.2 m × 0.8 m. The plants were pruned leaving four two-bud spurs per vine, whereas pest control and soil and canopy management followed standard local management practices, i.e. winter pruning, partial defoliation around cluster after veraison and fruit thinning.

Experimental design and data collection

In Site A, LAI measurements were performed on June 11 (Day of the Year, DOY = 162) and July 9 (DOY = 190) 2015 using a LAI-2000 optoelectronic sensor (LI-COR, Lincoln, Nebraska, USA) and following the tow-azimuth protocol (Welles & Norman, 1991, LI-COR 1992). The LAI measurements were performed in three different vigor areas of the vineyard: high (H1), medium (M1) and low (L1) areas (Fig. 1a, Site A). In each area, three adjacent portions of rows (3 rows \times 20 m each) were selected (total 75 vines). All three rows were included in LAI measurements as described in Caruso et al. (2017), whereas only the central row in each area was used for the determination of pruning weight (Fig. 1b, Site A). Fresh pruning weight (kg/linear meter of vine-row) was measured in February 2016 on a portion of 20 m consisting of four replicates (4 m each) per vigor group (Fig. 1b, Site A). The 50% of dry matter found on the total shoot biomass allowed fresh pruning weight to be converted into dry weight (Caruso, unpublished data). Phenological stages of beginning of flowering (61), fruit-set (71), beginning of bunch closure (77) and veraison (83) based on BBCH-scale stages (Lorenz et al., 1995) were observed on the field.

Daily maximum and minimum air temperature ($^{\circ}\text{C}$), precipitation (mm), global solar radiation (W m^{-2} then converted in $\text{MJ m}^{-2} \text{day}^{-1}$) and wind speed (m s^{-1}) were collected by a weather station sited 8 km away from the vineyard (Venturina, $43^{\circ} 1' 14.545$, $10^{\circ} 36' 22.23^{\circ}$ E). Soil texture, available nutrient content and percentage of organic matter were measured on soil samples collected in five zones and at two soil depths (0.25 and 0.50 m).

In Site B, field samplings were performed three times during the growing season: on June 26 (DOY = 177), August 8 (DOY = 220) and September 25 (DOY = 268) 2018 in two zones of the vineyard characterized by high (H2) and low (L2) plant vigor (Fig. 1a, Site B). The sampling areas comprised 39 Sentinel-2A pixels (10×10 m): 19 pixels were placed in H2 zone and the remaining 20 in the L2 zone. For each pixel, an average of 5 vines (min. 3–max. 9) were sampled (one plant every 10 plants) on the row along the field slope (Fig. 1b, 208 plants in total). fPAR and LAI were measured by AccuPAR, LP-80 Ceptometer (Decagon Devices, Inc., Pullman, Wash). The ceptometer was positioned along the row to directly estimate the above ($\text{PAR}_{\text{above}}$) and below ($\text{PAR}_{\text{below}}$) fraction of the PAR (López-Lozano & Casterad, 2013). The $\text{PAR}_{\text{above}}$ and $\text{PAR}_{\text{below}}$ were used for deriving the fraction of intercepted radiation $\left(1 - \frac{\text{fPAR}_{\text{below}}}{\text{fPAR}_{\text{above}}}\right)$ and LAI. The ceptometer measurements collected along the row were subsequently converted into canopy fPAR data as shown in López-Lozano and Casterad (2013). The canopy dimensions (i.e. height, width and length) were assessed on a total of 30 plants, randomly selected in the H2 and L2 zones of the vineyard (Fig. 1a, Site B). At harvest (25 September), the fresh fruit weight (kg plant^{-1}) was measured on 208 sampled plants (Fig. 1b, Site B). Dry fruits weight was estimated after drying fresh fruits at 80°C for 3 days, using 20 representative bunches from the sampled vines. All measurements (fPAR, LAI and fruits weight) were then averaged at pixel scale. The phenological phases of flowering, fruit-set and veraison were extracted from the Agroambiente regional website (<http://agroambiente.info.regione.toscana.it/>) in Fonterutoli area, assuming that maturity stage corresponds to harvest time.

Weather variables, Soil Water Content data (SWC , $\text{m}^3 \text{m}^{-3}$) and phenological observations were also collected. Daily maximum and minimum air temperature ($^{\circ}\text{C}$), precipitation (mm) and wind speed (m s^{-1}) were gathered by an automatic weather station sited 11 km away from the vineyard (weather station code: TOS11000087; TOS11000019; <https://www.sir.toscana.it/>). Global solar radiation ($\text{MJ m}^{-2} \text{day}^{-1}$) was estimated from air temperature according to Hargreaves and Samani (1982). SWC was sampled during 2018

in two pixels placed in H2 and L2 zone (Fig. 1a, Site B) at 15–20 cm depth using Decagon EC-5 sensors (Decagon Devices, 2010) with a frequency of 15 min and then aggregated at daily scale.

Image acquisition and processing

An Unmanned Aerial Vehicle (UAV) flight campaign was performed on June 26, 2018 in site B using the multirotor platform (Mikrokooper HiSystems GmbH, Moomerland, Germany, Di Gennaro et al., 2019). The flight plan was managed by the software Mikrokooper Tool (V2.20, HiSystems GmbH, Moomerland, Germany), which allows generating a route of waypoints as a function of the sensor field of view (FOV), the degree of overlapping between images and the ground resolution needed. The flight height was 50 m above ground level, achieving 0.03 m ground resolution and 80% of forward and lateral overlap. The images, used for the detection of vine canopy cover, were acquired by a Sony Cyber-shot DSC-QX100 RGB camera (Sony Corporation, Tokyo, Japan), which includes a CMOS Emor R sensor (20.2 megapixel) and a Carl Zeiss Vario-Sonnar T lens. The high resolution RGB images were recorded at noon under clear sky conditions. Subsequently, the images were mosaicked using Agisoft Photoscan Professional Edition 1.1.6 (Agisoft LLC, St. Petersburg, Russia), and processed using ArcGIS (ArcMap 10.3). Extraction of the vine canopy cover from RGB images was performed considering the color distribution curves of main elements in the vineyard (i.e. vegetation and background): a thresholding technique was applied on the green index to detect the plant canopy and thus extract the vegetation cover (Maselli et al., 2012). Moreover, the 2A product (surface reflectance) images of Sentinel-2A at 10×10 m resolution were acquired from the official Copernicus Open Access Hub (<https://scihub.copernicus.eu>). The available cloud-free Sentinel-2A images (179 and 219 day of year, DOY) closer to the field measurement campaign dates (DOY 177 and 219) were manually selected. Those images were subsequently processed using the raster package (version 2.8_19) in the R software environment (version 3.5.2) to extract the NDVI (Eq. 1, Rouse et al., 1974) in the 39 pixels of Site B. The NDVI values, ranging from −1 (deep water) to +1 (dense green vegetation), at fruit-set stage (DOY 177) were then used for spatially re-scaling on the vine canopy cover derived by the UAV flight and used to estimate fPAR data.

$$NDVI = \frac{NIR - RED}{NIR + RED}, \quad (1)$$

where NIR is the reflectance in the near-infrared band (760–900 nm) and RED is the reflectance in the red band (630–690 nm).

Forcing grapevine simulation model with fPAR data

The original version of UNIFI.GrapeML (Leolini et al., 2018a) simulates biomass accumulation at a daily time step, as a function of LAI and fPAR, which is then converted into biomass using the radiation use efficiency (RUE, g MJ⁻¹) approach as described in Bindi et al. (1997a, 1997b) for grapevine. The daily value of RUE is modulated according to CO₂ concentration and as a function of air temperature (Ritchie & Otter, 1985; Van Leuken & Seligman, 1987). The accumulated biomass is converted into transpired water using the transpiration efficiency coefficient (Soltani & Sinclair, 2012). The phenological model defines budbreak occurrence, which depends on the accumulation of chilling and

forcing units from a user-defined day of the year until the end of the eco-dormancy period. The development stages after budbreak are estimated using the forcing unit accumulation approach (Caffarra & Eccel, 2010). During the budbreak-flowering period, the biomass is entirely allocated into vegetative organs, whereas during fruit-set-harvest period it is partitioned into fruits, proportionally to daily increases in the harvest index (dHI/dT). The model also takes into account the effect of suboptimal temperatures around flowering, by introducing a yield-reducing temperature factor, as described by Farquhar and Caemmerer (1982) for photosynthesis.

In this study, the simulated LAI dynamic was adapted to reproduce the senescence process after veraison, thus separating the photosynthetically active green leaf area index (GLAI) from the total LAI. The GLAI trend was divided into three stages: in stage 1, the GLAI increases from budbreak to fruit-set. In stage 2, the GLAI remains constant up to veraison, after which it starts decreasing due to leaf senescence (stage 3). In the third stage, temperature and photoperiod modulate the impact of senescence as described in Delpierre et al. (2009) for deciduous trees (Bregaglio et al., 2016; Online Resource 1). The simulated fPAR dynamic, as previously described in Bindi et al. (1997a, 1997b), now follows this GLAI dynamic.

The simulation was initially performed without forcing the model with proximal and satellite RS data, in order to derive the maximum value of fPAR at fruit-set. This run allowed the trend of fPAR to be set (pre-run fPAR trend), which was derived as the ratio between the unforced daily fPAR ($fPAR_{iU}$) and the pre-run max fPAR ($\max[fPAR_{fruit-setU}]$). Subsequently, the values of LAI (Site A) and NDVI (Site B) at fruit-set stage were used to derive the fPAR at maximum vine canopy development, using two linear relationships. The maximum value of fPAR from RS sensors ($\max[fPAR_{fruit-setRS}]$) was then multiplied by the pre-run fPAR trend to obtain the daily dynamics of intercepted radiation (Eq. 2).

$$fPAR_i = \frac{fPAR_{iU}}{\max[fPAR_{fruit-setU}]} \cdot \max[fPAR_{fruit-setRS}]. \quad (2)$$

UNIFI.GrapeML model (Fig. 2) was coupled with UNIMI.SoilW component, which is a software library collecting models to simulate crop water uptake and redistribution in the soil profile (Donatelli et al., 2014; Leolini et al., 2018a). The ratio between available and total water holding capacity in one meter of the root zone (i.e. field capacity and wilting point) was used to compute a water stress index (0–1, 0 maximum stress, 1 no stress), which is a reducing factor of leaf area expansion and plant photosynthesis (Bindi et al., 1997a, 1997b, 2005). The minimum weather dataset required to drive the model includes daily data of maximum and minimum air temperature, global solar radiation and precipitation, other than the CO₂ atmospheric concentration.

Strategies for fPAR estimation

In Site A, LAI field measurements collected on DOY 162 and 190 were used for deriving LAI values on DOY 149 and 224 in all three vineyard vigor areas (H1, M1, L1) by using the LAI vs NDVI relationship found by Caruso et al. (2017) with the purpose of evaluating the LAI trend during the season.

Subsequently, the average LAI values measured on each vigor area at 162 DOY (fruit-set stage) were converted into fPAR data of the four corresponding replicates of the central row. fPAR data were derived by a linear regression obtained from ceptometer observations

Fig. 2 UNIFI.GrapeML workflow including the new implementations (red color). LeafFallDelPierre, LeafSenescence and LeafCycle are new models implemented for describing leaf development during the growing season on which fPAR is modulated. The implementation of the switch in the Intercepted radiation model allows the user to select between fPAR simulated by the model (fPAR model, ML) or fPAR derived by RS systems (fPAR RS). T_x daily maximum air temperature ($^{\circ}\text{C}$), T_n daily minimum air temperature ($^{\circ}\text{C}$), P precipitation (mm day^{-1}), GSR global solar radiation ($\text{MJ m}^{-2} \text{day}^{-1}$), CF Chilling-Forcing, GDD growing degree days ($^{\circ}\text{C day}^{-1}$), t resolution time

among these two variables in Site B ($fPAR = 0.149 \cdot LAI + 0.0585$, $r^2 = 0.94$). The four fPAR data extracted per vigor area were used to force the grapevine simulation model.

In Site B, fPAR was calculated from remotely-sensed NDVI values after detecting actual vine cover from the UAV flight. Given that grapevine canopies did not entirely cover the ground, a re-scaling procedure was applied on Sentinel-2A NDVI data in order to estimate the contribution of grapevine and grass cover. The correlation between the vine canopy cover extracted from all pixels of the UAV image and the related values of Sentinel-2A NDVI (Fig. 3, solid line) allowed the NDVI value to be derived, corresponding to full pixel coverage by vine canopy (when canopy cover is equal to 1, according to Maselli et al., 1998). Subsequently, the NDVI value at full canopy cover was thus re-scaled using the vine cover of each pixel to extrapolate the actual NDVI contributions due to vines ($NDVI_{Actual} = NDVI_{FullCC} \cdot CC$).

The resulting NDVI was then converted into fPAR using the generalized linear equation of Myneni and Williams (1994), which was successfully applied to other crops (e.g. Maselli et al., 2012 on olive tree; Eq. 3).

$$fPAR = 1.1638 \cdot NDVI - 0.1426, \quad (3)$$

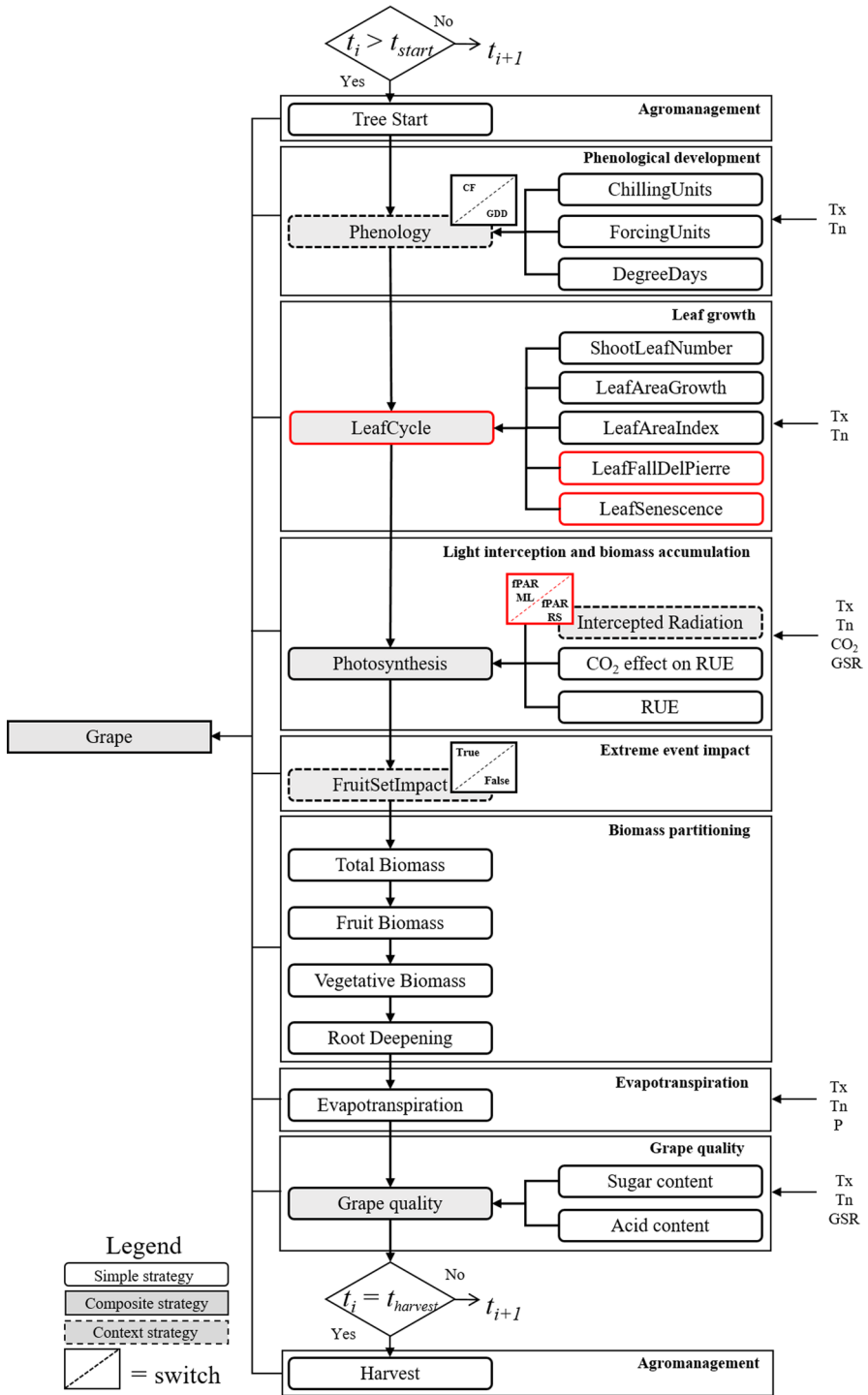
where fPAR ranges from 0 to 1.

Model parameterization and performance evaluation

The accuracy of the data assimilation methodology proposed in this study was evaluated comparing simulated outputs with the observations collected in the two study cases. In Site A, the UNIFI.GrapeML was forced using fPAR data directly estimated from proximal LAI observations in the field, whereas in Site B the model forcing was performed by using of NDVI-derived fPAR data from satellite RS platform.

The grapevine simulation model was calibrated for Sangiovese variety (Table S1 in Online Resource 2) in previous studies (Bindi et al., 1997a, 1997b, 2001a, 2001b, 2005; Leolini et al., 2019). In this work, only the parameters related to leaf area development (SLAE) and biomass partitioning (HI and HI_{cutoff}) were adjusted in order to improve model accuracy in simulating leaf area and fruit biomass (Table S1 in Online Resource 2). The information on vine training management (shoot number and planting density) was used for adjusting the simulation to the actual conditions of Site A and B.

Since the growth model does not explicitly consider the distribution of biomass in shoots and leaves, the weight of shoots at pruning for site A was obtained from simulated vegetative biomass by subtracting the weight of leaf biomass calculated using simulated leaf area and the specific leaf weight ($54.85 \text{ g dry weight m}^{-2}$, Palliotti et al., 2009). Dry matter partitioning towards the shoots after harvesting was considered negligible (Nendel & Kersebaum, 2004).



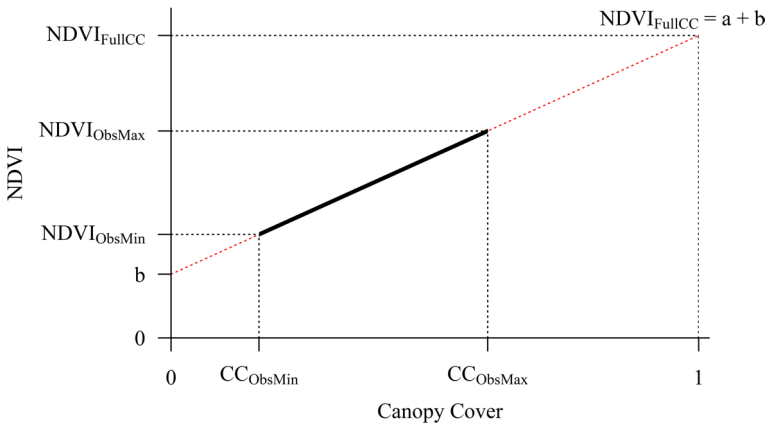


Fig. 3 Procedure of NDVI re-scaling based on the vine canopy cover in Site B. $NDVI_{ObsMax}$ and $NDVI_{ObsMin}$ are the maximum and minimum observed values of the NDVI extracted by Sentinel-2A image for all pixels, respectively. CC_{ObsMax} and CC_{ObsMin} are the maximum and minimum observed values of the canopy cover extracted by UAV image for all pixels, respectively. $NDVI_{FullCC}$ is the NDVI value at full vine canopy cover while a is the slope and b is the intercept of the linear regression

Model performances were evaluated using the Determination coefficient (r^2 , Eq. 4), Root Mean Squared Error (RMSE, Eq. 5) and Coefficient of Residual Mass (CRM, Eq. 6). The target variables for model evaluation were the shoot biomass in Site A and grapevine yield and water balance in Site B.

$$r^2 = 1 - \frac{\sum_{i=1}^n (O_i - P_i)^2}{\sum_{i=1}^n (O_i - \bar{O})^2}, \quad (4)$$

$$RMSE = \left[\sum_{i=1}^n \frac{(P_i - O_i)^2}{n} \right]^{0.5}, \quad (5)$$

$$CRM = \frac{\sum_{i=1}^n O_i - \sum_{i=1}^n P_i}{\sum_{i=1}^n O_i}, \quad (6)$$

where O_i is the observed value, \bar{O} is the average of the observed values, P_i is the predicted value, n is the number of observations.

Results

Grapevine model performance after forcing with fPAR derived from proximal LAI observations

UNIFI.GrapeML was able to reproduce the LAI development and shoot biomass accumulation during the 2015 growing season in Site A (Fig. 4). The LAI trend was compared to

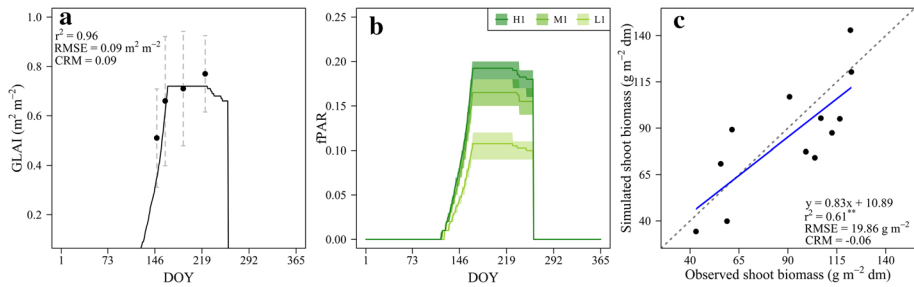


Fig. 4 **a** Simulated GLAI trend (solid line) and LAI observations (black dots) \pm standard deviation over the growing season in Site A. **b** Average fPAR (solid lines) and variability (colored shaded areas) seasonal trends in H1, M1 and L1 vigor areas. **c** Correlation between simulated and observed shoot biomass (g m^{-2} , dm dry matter) in all vineyard vigor areas (H1, M1, L1) at the end of the season. Significance level: ** $p < 0.01$ (Color figure online)

simulated GLAI showing satisfactory performances at field scale ($r^2 = 0.96$; $\text{RMSE} = 0.09$; $\text{CRM} = 0.09$; Fig. 4a). The forcing of UNIFI.GrapeML with the maximum fPAR value at fruit-set stage allowed the simulation to be re-initialized (Fig. 4b). The model was thus able to differentiate the trends of fPAR in areas of different vigor (H1, M1, L1) and to simulate shoot biomass at the end of the season ($r^2 = 0.61$; $\text{RMSE} = 19.86 \text{ g m}^{-2}$ dry matter; $\text{CRM} = -0.06$, Fig. 4c).

Grapevine model performance after forcing with fPAR derived from Sentinel-2A NDVI data

NDVI re-scaling and fPAR estimation from remote sensing imagery

The proposed procedure allowed the contribution of the grapevine and ground grass to the canopy cover to be discerned, by rescaling NDVI values derived from Sentinel-2A pixels with a single UAV image in Site B ($r^2 = 0.80$; Fig. 5a). The comparison between the original NDVI from Sentinel-2A and the actual NDVI contribution of vine canopies in each pixel of the experimental design is shown in Fig. 5b ($r^2 = 0.80$). The derived fPAR was thus compared to observed data of intercepted radiation measured by the ceptometer, showing satisfying accuracy at maximum canopy development ($r^2 = 0.83$; $\text{RMSE} = 0.04$; $\text{CRM} = -0.09$; Fig. 5c-June). On the contrary, a larger difference between NDVI-based and observed fPAR was found in August ($r^2 = 0.66$; $\text{RMSE} = 0.06$; $\text{CRM} = -0.20$; Fig. 5c-August). Finally, it is worth mentioning that the use of the re-scaling procedure increased the correlation between fPAR obtained from Sentinel 2A images and ceptometer measurements ($r^2 = 0.62$; $\text{RMSE} = 0.24$; $\text{CRM} = -1.23$; Fig. S1 in Online Resource 2).

Soil water content simulation

Soil water dynamic was accurately simulated in both L2 and H2 zones of Site B (L2 zone—pixel 29: $r^2 = 0.66$; $\text{RMSE} = 0.023 \text{ m}^3 \text{ m}^{-3}$; $\text{CRM} = 0.01$; H2 zone—pixel 8: $r^2 = 0.66$; $\text{RMSE} = 0.024 \text{ m}^3 \text{ m}^{-3}$; $\text{CRM} = 0$). The comparison of simulated and measured SWC data is shown in Figs. 6 and S2 in Online Resource 2. SWC was close to field capacity ($0.231 \text{ m}^3 \text{ m}^{-3}$) at the beginning and end of the season because of the high amount of precipitation occurring during the spring-winter period (January–May and November–December),

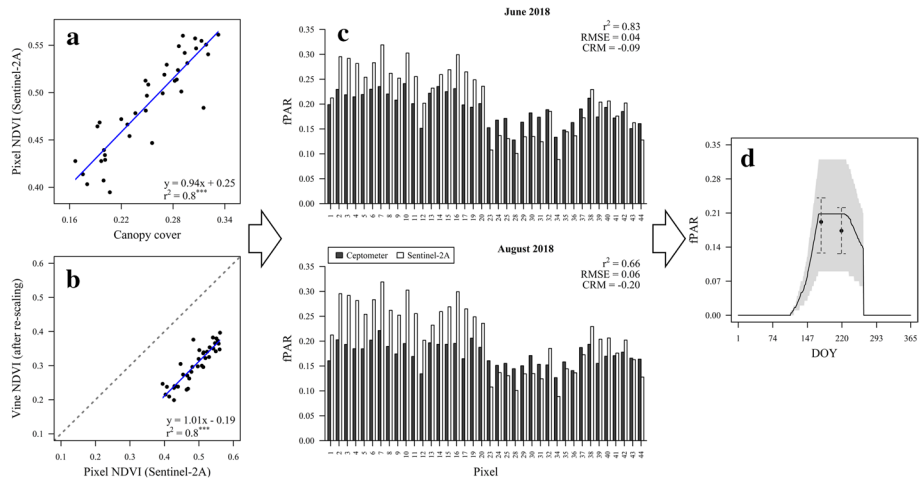


Fig. 5 **a** Correlation between vine canopy (from 0 to 1) and NDVI values (from 0 to 1) extracted for each pixel of Sentinel-2A image at fruit-set stage in Site B. **b** Correlation between NDVI values (from 0 to 1) of each pixel in Sentinel-2A image and the NDVI values of vine canopies (from 0 to 1) after re-scaling NDVI on the vine canopy cover (from 0 to 1) of each pixel. **c** Comparison between Sentinel-2A (DOY 179; white bars) and Ceptometer-derived (DOY 177; black bars) fPAR in June 2018 (top) and August 2018 (DOY 219; bottom). **d** Average (continuous line) and variability (shaded area) of the seasonal trend of the fraction of intercepted radiation simulated using UNIFI.GrapeML in Site B. The points with whiskers represent the average value and variability of the fPAR distribution measured with a ceptometer in June and August 2018 in each pixel of the experimental design. Significance level: *** $p < 0.001$

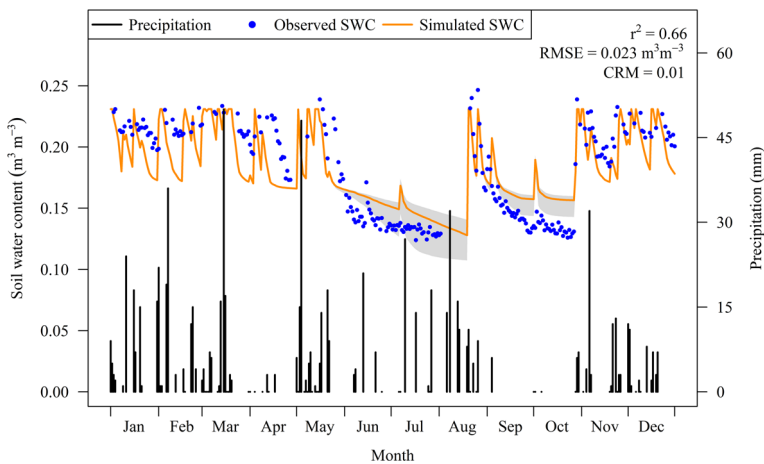


Fig. 6 Soil water content dynamics during 2018 in the low vigor area of Site B. The observed and simulated values of the soil water content ($\text{m}^3 \text{m}^{-3}$) for the pixel (number 29, see Fig. 1a, Site B) where soil water sensors were placed are reported in blue (points) and orange (continuous line). The shaded area represents the soil water content variability after forcing the model with fPAR data in all pixels of the experimental design. The secondary y-axis shows the amount of daily precipitation (mm; solid black line) (Color figure online)

whereas it decreased during summer until the beginning of autumn when wilting point ($0.130 \text{ m}^3 \text{ m}^{-3}$) was reached as a consequence of root water uptake in the drought period. The simulated SWC matched the data measured by soil water probes positioned in L2 vigor pixel (SWCS2 in Fig. 1a, Site B; Fig. 6). The forcing with remotely-sensed fPAR allowed the simulation model to differentiate the plant growth and transpiration in each pixel and to adequately represent the variability of SWC at pixel scale (Figs. 6, S2 in Online Resource 2—shaded areas). The minimum simulated SWC ranges from 0.11 to $0.15 \text{ m}^3 \text{ m}^{-3}$ at DOY 205 (23 July), depending on the plants’ vigor in the different pixels of Site B.

Grapevine yield simulation

UNIFI.GrapeML was able to accurately reproduce the GLAI value at fruit-set stage ($0.90 \text{ m}^2 \text{ m}^{-2}$ simulated vs $0.89 \text{ m}^2 \text{ m}^{-2}$ observed) at field level. The model was also able to reproduce the variability of grapevine yield at Sentinel-2A pixel scale of Site B ($r^2=0.47$; $\text{RMSE}=75.52 \text{ dry matter g m}^{-2}$; $\text{CRM}=0$; Fig. 7a), after calibrating harvest index according to measurements (51% of the total plant biomass partitioned to the fruit). The larger fruit biomass production in the upper side of the vineyard was determined by higher plant vigor. This higher plant vigor led to higher light interception as revealed by the field observations ($\text{RMSE}=0.05$; mean daily intercepted radiation from bud-break to maturity= 0.18 , $\text{RMSE}=92.16 \text{ g m}^{-2}$ dry matter). On the contrary, a lower fruit biomass production was determined by a decreased plant vigor in the lower side of the vineyard. Similarly, a low plant vigor corresponded to decreased light interception (intercepted radiation $\text{RMSE}=0.02$, mean daily intercepted radiation from bud-break to maturity= 0.11 , grapevine yield $\text{RMSE}=59.45 \text{ g m}^{-2}$ dry matter, Figs. 7b, S3 in Online Resource 2).

Discussion

The use of state variables (e.g. fPAR or LAI) obtained from remote sensing to drive crop simulation models allows the variability of plant growth and development processes to be captured at sub-field scale and this approach is widely described in the literature

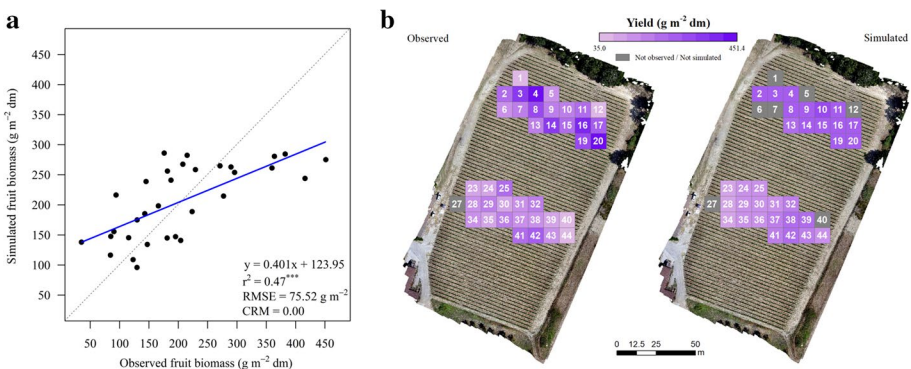


Fig. 7 **a** Correlation between observed and simulated values of fruit biomass (g m^{-2} , dm =dry matter) obtained forcing UNIFI.GrapeML with NDVI-derived fPAR data in Site B. **b** Comparison between observed and simulated yield (g m^{-2} dm) in high and low productivity zones of the vineyard. Significance level: *** $p < 0.001$

(e.g. Ginaldi et al., 2019; Huang et al., 2019; Jin et al., 2018). The availability of satellite data at a time resolution comparable to the time step of the simulation model is a prerequisite for a model forcing approach (Jin et al., 2018). This implies the use of multi-temporal data that, while increasing the accuracy of the simulations, can reduce the model usability for real-time monitoring operations (Wang et al., 2014; Zhou et al., 2017). Furthermore, satellite revisiting frequency is usually coarser than the model time step, therefore post-processing approaches must be applied to reduce this gap (Huang et al., 2019; Jin et al., 2018). As an example, Moriondo et al. (2007) derived fPAR on a daily time step by linearly interpolating the original NDVI data obtained from NOAA-AVHRR to drive the Cropsyst simulation model (Stöckle et al., 2003).

The challenge faced in this study consisted of finding a compromise between simulation accuracy and input requirements for estimating grapevine growth and harvested yield, testing the feasibility of a single satellite image joined with a high resolution RGB image to estimate vine leaf area growth during the season. This simplification is intended to foster the operational implementation of the proposed methodology for real-time monitoring of vine growth and development. Specifically, the forcing approach focused on the sole use of fPAR data obtained at fruit-set to drive crop model simulation over the entire growing season. This stage corresponds to the time when canopy development and the relevant light interception reach their maximum value during the season (Munitz et al., 2020; Orlandini et al., 2008, Online Resource 1), considered as the best moment for capturing the vine growth variability at sub-field scale. Previous studies on both annual (Huang et al., 2015; Panigrahy et al., 2012) and woody crops (Bai et al., 2019) already pointed out that model forcing with leaf area detected at maximum vegetative development plays a major role in improving the simulation accuracy with respect to leaf areas obtained in other phenological stages. In this sense, the use of Sentinel-2 imagery having a more frequent updating of the remotely sensed information due to the high revisiting frequency of this satellite mission (Maselli et al., 2020), allows a more accurate estimation of when the plant reaches maximum vigor.

After fruit-set, the simulation continues without further assimilating RS data, relying on the crop model algorithms that describe canopy dynamics. These consider that leaf area growth stops after fruit-set, and starts decreasing after veraison as a consequence of senescence processes (Munitz et al., 2020; Figs. 4, 5; Online Resource 1), which are triggered by lowering temperatures and reducing day length (Delpierre et al., 2009). This accounts for the differences in seasonal fPAR dynamics simulated in Site A, where higher temperatures during the veraison-maturity stage smoothed the senescence process with respect to Site B, where lower temperatures accelerated the process (Figs. 4, 5). In Site A, fPAR at fruit-set, estimated from measured LAI, allowed the model to reproduce the spatial variability of shoot biomass growth, proving the reliability of the proposed methodology to estimate early the biomass accumulation expressed as final shoot biomass (Fig. 1a).

The approach proved to be valid using NDVI-derived fPAR from satellite RS data as forcing factor at pixel scale in Site B, even given the difficulties in distinguishing the actual contribution of crop canopy cover and plant inter-row components to the signal perceived by satellite platforms (Battista et al., 2016). In this regard, one of the main results of this study is the application and validation of a methodology to disentangle the contribution of vine canopy and the inter-row to the NDVI value from RS, thus enabling the effective integration of satellite data into a crop growth model. The proposed approach, originally developed by Maselli (2001) for different soil cover classes, which was already successfully applied to olive orchards (Maselli et al., 2012; Leolini et al., 2022), is based on the use of maps that spatially describe the distribution of fraction cover. A single high-resolution

UAV image (~3 cm) acquired around fruit-set (DOY 179) was thus used in site B to segment the grapevine canopy cover and to evaluate the actual contribution of grapevine plants to the NDVI signal at single pixel scale (Fig. 5a). The linear relationship between plant canopy cover and the NDVI values obtained at fruit-set allowed us to extrapolate the NDVI contribution of the vine canopies and to derive actual fPAR data relevant to grapevine. The re-scaling of NDVI at Sentinel-2A pixel scale, compared to the direct use of raw NDVI values (higher r^2 and lower RMSE), is thus a fundamental step at this stage which allows to improve the estimation of the spatial variability of fPAR. The use of this simple strategy allowed to satisfactorily distinguish the variability in fPAR existing between two vigor areas of Site B at fruit-set stage (Fig. 5c–June) even though simulation accuracy decreased in August (DOY 219), when simulated fPAR was generally overestimated (Fig. 5c–August).

Despite more complex approaches having been demonstrated to be more effective in detecting plant vigor and biophysical parameters at sub-field level (Khaliq et al., 2019; Matese et al., 2015; Sozzi et al., 2020), the need for high-resolution images (e.g. UAVs) and the time-consuming data post-processing make these strategies less affordable for crop monitoring. Moreover, the empirical approaches generally used for directly estimating the actual crop state (e.g. vigor, yield, etc.) through remotely sensed VIs and statistical or deep learning methods (Arab et al., 2021; Ballesteros et al., 2020; Di Gennaro et al., 2019; Matese & Di Gennaro, 2021; Sun et al., 2017) cannot provide information on the causes that may lead to a reduction in harvested yield. By contrast, the dynamic of growth processes is fully considered in process-based models where crop physiological responses are modeled in relation to the variability of climate, soil and management conditions and environmental stresses (e.g. water stress; Bindi et al., 1997a, 1997b; Brisson et al., 2003). Therefore, a grapevine simulation model, which explicitly reproduces the crop physiological processes, may indeed account for the effect of agro-management practices and environmental conditions (e.g. heat and water stress) on vine growth and yield (Figs. 7, S3 in Online Resource 2). Finally, in spite of the bias in fPAR detection, the approach faithfully reproduced soil water dynamics during the season considering two distinct areas where soil water sensors were positioned (Figs. 6, S2 in Online Resource 2), other than being able to satisfactorily capture the spatial variability of final yield, even without a specific model calibration on these experiments.

However, despite the good model performances in reproducing soil water dynamics, vegetative growth and final yield, some drawbacks of the proposed approach can be highlighted. From a purely operational point of view, the model can be forced only after evaluation of the fraction cover of vine canopies, which is needed to rescale NDVI and to extract fPAR at the fruit-set stage. While this fraction can be assumed almost constant in time and space in a mature olive grove (Leolini et al., 2022; Maselli et al., 2012; Moriondo et al., 2019), this does not hold in a vineyard and must be evaluated seasonally. This implies the retrieval of detailed maps to drive NDVI signal partitioning (Fig. 3, Eq. 3) thus resulting in a bottleneck for the development of an automated service for estimating growth and development processes. The use of a single high-resolution image for detecting the vine fraction cover at maximum canopy development may avoid the huge, and often not feasible, model input requirements during the season. However, this implies that, after this stage, the dynamics of the state variable will be described according to the specific modeling approach adopted. In this sense, the overestimation of fPAR in August is likely related to the increase of simulated leaf area from fruit-set to veraison stage (Fig. 5d, Fig. S1, Online Resource 1). The LAI, and consequently the fPAR of vine plants, in fact, can vary during a growing season due to both phenological development and environmental factors, such as

thermal and water limitations. The bias between estimated and observed fPAR may therefore be ascribed to a possible reduction in leaf area due to leaf loss following high water stress (Chacón-Vozmediano et al., 2020; Picón-Toro et al., 2012), which is not accounted for in the model and would require a specific algorithm.

Besides the intrinsic features of the variety, vegetative and reproductive growth is indeed strongly related to environmental stresses and management practices. In this study, different planting density and shoot numbers have been taken into account to represent the different vegetative and fruit growth conditions of Sangiovese in Site A and B (Table S1 in Online Resource 2). However, the model simulates the dynamics of fruit growth as a fixed percentage of daily accumulated biomass based on a proportional biomass increase with respect to the radiation intercepted by the canopy (Bindi et al., 1997a, 1997b; Sun et al., 2017). This fixed ratio may be reduced according to suboptimal temperatures at fruit-set (Leolini et al., 2018a). Differently to other approaches that focused on source-sink relationships for describing carbon partitioning among vegetative and reproductive plant organs (Cola et al., 2014; Vivin et al., 2002; Wermelinger et al., 1991), the model used here does not consider these plant strategies in biomass partitioning. This implies that the changes occurring in the potential demand of a specific pool and the way this mechanism can alter the carbon allocation to plant organs during the season were not taken into account. Thus, daily carbon partitioning being independent from the demand of a specific organ, no competition for carbon from the different organs was assumed, and the effect of unfavorable climate conditions and/or agro-management practices (e.g. fruit and shoot thinning) which may stimulate the assimilates partitioning towards other organ sinks (Keller et al., 2005; Naor et al., 2002) was also discarded. This forcing approach allowed a satisfactory yield estimation to be provided, especially in low vigor areas (Fig. 6). The lower model performances in the high vigor area can be related to the saturation of NDVI when LAI increases. In agreement with Junges et al. (2019), the increase of NDVI with respect to the increase of leaf area suggests that NDVI shows a logarithmic behaviour rather than linear for LAI higher than 1, which prevents to highlight differences among plant vigor in vineyards. This issue might be overcome by the adoption of non-linear vegetation indices which are generally less affected by canopy variation and background effects (e.g. GEMI, MSAVI, OSAVI, etc.), thus being less sensitive to saturation and showing up the differences in high vine vigor zones (Haboudane et al., 2004; Leolini et al., 2022; Pinty & Verstraete, 1992; Rondeaux et al., 1996).

Despite the abovementioned simplifications, the study represents the first attempt to force a vineyard simulation model with RS data, in the absence of an adequate spatial resolution for vine canopy representation, with the purpose of improving vine growth and yield simulation in a system characterized by plant and inter-row layers. The approach thus lays the basis for a Decision Support System to help winegrowers consortiums and cooperatives to timely identify the most adequate management practices fostering the increase of grapevine yield, and thus their competitiveness on the wine market.

Conclusions

This study focused on the forcing of an existing grapevine model (UNIFI.GrapeML) with fPAR data at fruit-set stage in order to evaluate the variability of biomass accumulation and fruit production at sub-field level in two Tuscan vineyards.

The results indicate that the grapevine model forced with fPAR data from proximal sensing allowed vine biomass accumulation variability at sub-field level to be properly reproduced in Site A, resulting in an effective methodology for early prediction of harvested yield. This strategy was then applied in Site B using fPAR data derived from satellite imagery, showing satisfactory performances in reproducing sub-field yield variability. In this last study case, the adoption of the strategy for disentangling the contribution of the vegetation index among vine rows and inter-rows proved to be a crucial factor for the success of the methodology.

Despite further model refinements to address specific vineyard managements being needed, the application of UNIFI.GrapeML, with a limited number of RS-derived inputs represents the starting point to set up a decision support system to optimize vineyard production and limit within-field yield variability.

Supplementary Information The online version contains supplementary material available at <https://doi.org/10.1007/s11119-022-09970-8>.

Acknowledgements The authors acknowledge the Clim4Vitis project ‘Climate change impact mitigation for European viticulture: knowledge transfer for an integrated approach’, funded by the European Union’s Horizon 2020 Research and Innovation Programme, under Grant Agreement No. 810176 that supported this study. This research received support from the AgriDigit-Agromodelli project (DM n. 36502 of 20/12/2018), funded by the Italian Ministry of Agricultural, Food and Forestry Policies. The authors also gratefully acknowledge Castello di Fonterutoli—Marchesi Mazzei Spa Agricola and Bulichella farm for having hosted the experimental activities and Andrea Berton (CNR-IFC) for technically supporting the UAV data acquisition.

Author contributions Conceptualization: LL, MM, SC-A, SB, FG. Methodology: LL, MM, SB, FG, SC-A, FM; Resources: GC, GP, SFDG, AM, LL, MM, SC-A. Supervision: MB, MM. Writing—original draft: LL, MM. Writing—review & editing: LL, MM, SB, FG, SC-A, FM, GC, GP, SB, SFDG, AM, MB.

Funding Open access funding provided by Università degli Studi di Firenze within the CRUI-CARE Agreement.

Declarations

Conflict of interest Authors declare no conflict of interest.

Open Access This article is licensed under a Creative Commons Attribution 4.0 International License, which permits use, sharing, adaptation, distribution and reproduction in any medium or format, as long as you give appropriate credit to the original author(s) and the source, provide a link to the Creative Commons licence, and indicate if changes were made. The images or other third party material in this article are included in the article’s Creative Commons licence, unless indicated otherwise in a credit line to the material. If material is not included in the article’s Creative Commons licence and your intended use is not permitted by statutory regulation or exceeds the permitted use, you will need to obtain permission directly from the copyright holder. To view a copy of this licence, visit <http://creativecommons.org/licenses/by/4.0/>.

References

- Arab, S. T., Noguchi, R., Matsushita, S., & Ahamed, T. (2021). Prediction of grape yields from time-series vegetation indices using satellite remote sensing and a machine-learning approach. *Remote Sensing Applications: Society and Environment*, 22, 100485.
- Arnó, J., Martínez Casanovas, J. A., Ribes Dasi, M., & Rosell, J. R. (2009). Review: Precision viticulture. Research topics, challenges and opportunities in site-specific vineyard management. *Spanish Journal of Agricultural Research*, 7(4), 779. <https://doi.org/10.5424/sjar/2009074-1092>

- Bai, T., Zhang, N., Mercatoris, B., & Chen, Y. (2019). Improving jujube fruit tree yield estimation at the field scale by assimilating a single Landsat remotely-sensed LAI into the WOFOST Model. *Remote Sensing*, *11*(9), 1119. <https://doi.org/10.3390/rs11091119>
- Ballesteros, R., Intrigliolo, D. S., Ortega, J. F., Ramírez-Cuesta, J. M., Buesa, I., & Moreno, M. A. (2020). Vineyard yield estimation by combining remote sensing, computer vision and artificial neural network techniques. *Precision Agriculture*, *21*, 1242–1262.
- Barbera, G., & Cullotta, S. (2016). The traditional mediterranean polycultural landscape as cultural heritage: Its origin and historical importance, its agro-silvo-pastoral complexity and the necessity for its identification and inventory. In M. Agnoletti & F. Emanuelli (Eds.), *Biocultural diversity in Europe* (pp. 21–48). Springer.
- Basso, B., Ritchie, J. T., Pierce, F. J., Braga, R. P., & Jones, J. W. (2001). Spatial validation of crop models for precision agriculture. *Agricultural Systems*, *68*(2), 97–112. [https://doi.org/10.1016/S0308-521X\(00\)00063-9](https://doi.org/10.1016/S0308-521X(00)00063-9)
- Battista, P., Chiesi, M., Rapi, B., Romani, M., Cantini, C., Giovannelli, A., Cocozza, C., Tognetti, R., & Maselli, F. (2016). Integration of ground and multi-resolution satellite data for predicting the water balance of a Mediterranean two-layer agro-ecosystem. *Remote Sensing*, *8*, 731. <https://doi.org/10.3390/rs8090731>
- Biasi, R., Brunori, E., Ferrara, C., & Salvati, L. (2019). Assessing impacts of climate change on phenology and quality traits of *Vitis vinifera* L.: The contribution of local knowledge. *Plants*, *8*(5), 121. <https://doi.org/10.3390/plants8050121>
- Bindi, M., Bellesi, S., Orlandini, S., Fibbi, L., Moriondo, M., & Sinclair, T. (2005). Influence of water deficit stress on leaf area development and transpiration of Sangiovese grapevines grown in pots. *American Journal of Enology and Viticulture*, *56*(1), 68–72.
- Bindi, M., Fibbi, L., Lanini, M., & Miglietta, F. (2001a). Free air CO₂ enrichment (FACE) of grapevine (*Vitis vinifera* L.): I. Development and testing of the system for CO₂ enrichment. *European Journal of Agronomy*, *14*(2), 135–143. [https://doi.org/10.1016/S1161-0301\(00\)00092-7](https://doi.org/10.1016/S1161-0301(00)00092-7)
- Bindi, M., Fibbi, L., & Miglietta, F. (2001b). Free Air CO₂ enrichment (FACE) of grapevine (*Vitis vinifera* L.): II. Growth and quality of grape and wine in response to elevated CO₂ concentrations. *European Journal of Agronomy*, *14*(2), 145–155. [https://doi.org/10.1016/S1161-0301\(00\)00093-9](https://doi.org/10.1016/S1161-0301(00)00093-9)
- Bindi, M., Miglietta, F., Gozzini, B., Orlandini, S., & Seghi, L. (1997a). A simple model for simulation of growth and development in grapevine (*Vitis vinifera* L.) I. Model description. *Vitis*, *36*, 67–71.
- Bindi, M., Miglietta, F., Gozzini, B., Orlandini, S., & Seghi, L. (1997b). A simple model for simulation of growth and development in grapevine (*Vitis vinifera* L.) II. Model validation. *Vitis*, *36*(2), 73–76.
- Bregaglio, S., Orlando, F., Forni, E., De Gregorio, T., Falzoi, S., Boni, C., Pisetta, M., & Confalonieri, R. (2016). Development and evaluation of new modelling solutions to simulate hazelnut (*Corylus avellana* L.) growth and development. *Ecological Modelling*, *329*, 86–99. <https://doi.org/10.1016/j.ecolmodel.2016.03.006>
- Brisson, N., Gary, C., Justes, E., Roche, R., Mary, B., Ripoche, D., Zimmer, D., Sierra, J., Bertuzzi, P., Burger, P., Bussiere, F., Cabidoche, Y. M., Cellier, P., Debaeke, P., Gaudillere, J. P., Henault, C., Maraux, F., Seguin, B., & Sinoquet, H. (2003). An overview of the crop model STICS. *European Journal of Agronomy*, *18*(3–4), 309–332.
- Brook, A., De Micco, V., Battipaglia, G., Erbaggio, A., Ludeno, G., Catapano, I., & Bonfante, A. (2020). A smart multiple spatial and temporal resolution system to support precision agriculture from satellite images: Proof of concept on Aglianico vineyard. *Remote Sensing of Environment*, *240*, 111679. <https://doi.org/10.1016/j.rse.2020.111679>
- Caffarra, A., & Eccel, E. (2010). Increasing the robustness of phenological models for *Vitis vinifera* cv. Chardonnay. *International Journal of Biometeorology*, *54*, 255–267. <https://doi.org/10.1007/s00484-009-0277-5>
- Caruso, G., Tozzini, L., Rallo, G., Primicerio, J., Moriondo, M., Palai, G., & Gucci, R. (2017). Estimating biophysical and geometrical parameters of grapevine canopies ('Sangiovese') by an unmanned aerial vehicle (UAV) and VIS-NIR cameras. *Vitis*, *56*(2), 63–70.
- Chacón-Vozmediano, J. L., Martínez-Gascueña, J., García-Navarro, F. J., & Jiménez-Ballesta, R. (2020). Effects of water stress on vegetative growth and 'Merlot' grapevine yield in a semi-arid Mediterranean climate. *Horticulturae*, *6*(4), 95.
- Challinor, A. J., Wheeler, T. R., Craufurd, P. Q., Slingo, J. M., & Grimes, D. I. F. (2004). Design and optimisation of a large-area process-based model for annual crops. *Agricultural and Forest Meteorology*, *124*(1–2), 99–120. <https://doi.org/10.1016/j.agrformet.2004.01.002>
- Cinat, P., Di Gennaro, S. F., Berton, A., & Matese, A. (2019). Comparison of unsupervised algorithms for Vineyard Canopy segmentation from UAV multispectral images. *Remote Sensing*, *11*(9), 1023.

- Clevers, J. G. P. W., Büker, C., van Leeuwen, H. J. C., & Bouman, B. A. M. (1994). A framework for monitoring crop growth by combining directional and spectral remote sensing information. *Remote Sensing of Environment*, 50(2), 161–170. [https://doi.org/10.1016/0034-4257\(94\)90042-6](https://doi.org/10.1016/0034-4257(94)90042-6)
- Clevers, J., Vonder, O., Jongschaap, R., Desprats, J. F., King, C., Prévot, L., & Bruguier, N. (2002). Using SPOT data for calibrating a wheat growth model under Mediterranean conditions. *Agronomie*, 22(6), 687–694.
- Cola, G., Mariani, L., Salinari, F., Civardi, S., Bernizzoni, F., Gatti, M., & Poni, S. (2014). Description and testing of a weather-based model for predicting phenology, canopy development and source–sink balance in *Vitis vinifera* L. cv. Barbera. *Agricultural and Forest Meteorology*, 184, 117–136.
- Decagon Devices. (2010). *Soil moisture sensors user's manual* (p. 29). Vernier.
- Delpierre, N., Dufréne, E., Soudani, K., Ulrich, E., Cecchini, S., Boé, J., & François, C. (2009). Modelling interannual and spatial variability of leaf senescence for three deciduous tree species in France. *Agricultural and Forest Meteorology*, 149(6–7), 938–948.
- Di Gennaro, S. F., & Matese, A. (2020). Evaluation of novel precision viticulture tool for canopy biomass estimation and missing plant detection based on 2.5 D and 3D approaches using RGB images acquired by UAV platform. *Plant Methods*, 16(1), 1–12.
- Di Gennaro, S. F., Toscano, P., Cinat, P., Berton, A., & Matese, A. (2019). A low-cost and unsupervised image recognition methodology for yield estimation in a vineyard. *Frontiers in Plant Science*, 10, 1–13. <https://doi.org/10.3389/fpls.2019.00559>
- Donatelli, M., Bregaglio, S., Confalonieri, R., De Mascellis, R., & Acutis, M. (2014). A generic framework for evaluating hybrid models by reuse and composition—A case study on soil temperature simulation. *Environmental Modelling & Software*, 62, 478–486. <https://doi.org/10.1016/j.envsoft.2014.04.011>
- Fang, H., Liang, S., & Hoogenboom, G. (2011). Integration of MODIS LAI and vegetation index products with the CSM-CERES-Maize model for corn yield estimation. *International Journal of Remote Sensing*, 32(4), 1039–1065. <https://doi.org/10.1080/01431160903505310>
- Fang, H., Liang, S., Hoogenboom, G., Teasdale, J., & Cavigelli, M. (2008). Corn-yield estimation through assimilation of remotely sensed data into the CSM-CERES-Maize model. *International Journal of Remote Sensing*, 29(10), 3011–3032. <https://doi.org/10.1080/01431160701408386>
- FAO/IIASA/ISRIC/ISSCAS/JRC. (2012). *Harmonized world soil database (version 1.2)*. FAO.
- Farquhar, G. D., & von Caemmerer, S. (1982). Modelling of photosynthetic response to environmental conditions. *Physiological Plant Ecology*. https://doi.org/10.1007/978-3-642-68150-9_17
- Gilardelli, C., Stella, T., Confalonieri, R., Ranghetti, L., Campos-Taberner, M., García-Haro, F. J., & Boschetti, M. (2019). Downscaling rice yield simulation at sub-field scale using remotely sensed LAI data. *European Journal of Agronomy*, 103, 108–116.
- Ginaldi, F., Bajocco, S., Bregaglio, S., & Cappelli, G. (2019). Spatializing crop models for sustainable agriculture. In M. Farooq & M. Pisante (Eds.), *Innovations in sustainable agriculture* (pp. 599–619). Springer.
- Guo, C., Zhang, L., Zhou, X., Zhu, Y., Cao, W., Qiu, X., Cheng, T., & Tian, Y. (2018). Integrating remote sensing information with crop model to monitor wheat growth and yield based on simulation zone partitioning. *Precision Agriculture*, 19(1), 55–78. <https://doi.org/10.1007/s11119-017-9498-5>
- Haboudane, D., Miller, J. R., Pattey, E., Zarco-Tejada, P. J., & Strachan, I. B. (2004). Hyperspectral vegetation indices and novel algorithms for predicting green LAI of crop canopies: Modeling and validation in the context of precision agriculture. *Remote Sensing of Environment*, 90(3), 337–352.
- Hannah, L., Roehrdanz, P. R., Ikegami, M., Shepard, A. V., Shaw, M. R., Tabor, G., et al. (2013). Climate change, wine, and conservation. *Proceedings of the National Academy of Sciences of the United States of America*, 110(17), 6907–6912. <https://doi.org/10.1073/pnas.1210127110>
- Hargreaves, G. H., & Samani, Z. A. (1982). Estimating potential evapotranspiration. *Journal of the Irrigation and Drainage Division*, 108(3), 225–230.
- Huang, J., Gómez-Dans, J. L., Huang, H., Ma, H., Wu, Q., Lewis, P. E., Liang, S., Chen, Z., Xue, X., Wu, Y., Zhao, F., Wang, J., & Xie, X. (2019). Assimilation of remote sensing into crop growth models: Current status and perspectives. *Agricultural and Forest Meteorology*, 276, 107609.
- Huang, J., Ma, H., Su, W., Zhang, X., Huang, Y., Fan, J., & Wu, W. (2015). Jointly assimilating MODIS LAI and et products into the SWAP model for winter wheat yield estimation. *Journal of Selected Topics in Applied Earth Observations and Remote Sensing*, 8, 4060–4071.
- Jin, X., Kumar, L., Li, Z., Feng, H., Xu, X., Yang, G., & Wang, J. (2018). A review of data assimilation of remote sensing and crop models. *European Journal of Agronomy*, 92, 141–152.
- Junges, A. H., Fontana, D. C., & Lampugnani, C. S. (2019). Relationship between the normalized difference vegetation index and leaf area in vineyards. *Bragantia*, 78, 297–305.
- Keller, M., Mills, L. J., Wample, R. L., & Spayd, S. E. (2005). Cluster thinning effects on three deficit-irrigated *Vitis vinifera* cultivars. *American Journal of Enology and Viticulture*, 56(2), 91–103.

- Khaliq, A., Comba, L., Biglia, A., Ricauda Aimonino, D., Chiaberge, M., & Gay, P. (2019). Comparison of satellite and UAV-based multispectral imagery for vineyard variability assessment. *Remote Sensing*, *11*(4), 436.
- Koppen, W. D. (1936). Das geographische system der klimat. *Handbuch der Klimatologie*, *46*, 46. <https://doi.org/10.2307/200498>
- Leolini, L., Bregaglio, S., Moriondo, M., Ramos, M. C., Bindi, M., & Ginaldi, F. (2018a). A model library to simulate grapevine growth and development: Software implementation, sensitivity analysis and field level application. *European Journal of Agronomy*, *99*, 92–105. <https://doi.org/10.1016/j.eja.2018.06.006>
- Leolini, L., Moriondo, M., Fila, G., Costafreda-Aumedes, S., Ferrise, R., & Bindi, M. (2018b). Late spring frost impacts on future grapevine distribution in Europe. *Field Crops Research*, *222*, 197–208. <https://doi.org/10.1016/j.fcr.2017.11.018>
- Leolini, L., Moriondo, M., Romboli, Y., Gardiman, M., Costafreda-Aumedes, S., Costafreda-Aumedes, S., Garcia de Cortazar-Atauri, I., Bindi, M., Granchi, L., & Brillì, L. (2019). Modelling sugar and acid content in Sangiovese grapes under future climates: An Italian case study. *Climate Research*, *78*(3), 211–224. <https://doi.org/10.3354/cr01571>
- Leolini, L., Moriondo, M., Rossi, R., Bellini, E., Brillì, L., López-Bernal, Á., Santos, J. A., Fraga, H., Bindi, M., Dibari, C., & Costafreda-Aumedes, S. (2022). Use of Sentinel-2 derived vegetation indices for estimating fPAR in olive groves. *Agronomy*, *12*(7), 1540. <https://doi.org/10.3390/agronomy12071540>
- Li-Cor, I. (1992). *LAI-2000 plant canopy analyzer instruction manual*. Lincoln, Nebraska: LI-COR Inc.
- López-Lozano, R., & Casterad, M. A. (2013). Comparison of different protocols for indirect measurement of leaf area index with ceptometers in vertically trained vineyards. *Australian Journal of Grape and Wine Research*, *19*(1), 116–122. <https://doi.org/10.1111/ajgw.12005>
- Lorenz, D. H., Eichhorn, K. W., Bleiholder, H., Klose, R., Meier, U., & Weber, E. (1995). Growth stages of the grapevine: Phenological growth stages of the grapevine (*Vitis vinifera* L. ssp. *vinifera*)—Codes and descriptions according to the extended BBCH scale. *Australian Journal of Grape and Wine Research*, *1*(2), 100–103.
- Mabrouk, H., Sinoquet, H., & Carbonneau, A. (1997). Canopy structure and radiation regime in grapevine. I. Modeling radiation interception and distribution inside the canopy. *Vitis*, *36*(3), 125–132.
- Maselli, F. (2001). Definition of spatially variable spectral end-members by locally calibrated multivariate regression analyses. *Remote Sensing of Environment*, *75*, 29–38.
- Maselli, F., Angeli, L., Battista, P., Fibbi, L., Gardin, L., Magno, R., Rapi, B., & Chiesi, M. (2020). Evaluation of Terra/Aqua MODIS and Sentinel-2 MSI NDVI data for predicting actual evapotranspiration in Mediterranean regions. *International Journal of Remote Sensing*, *41*(14), 5186–5205.
- Maselli, F., Argenti, G., Chiesi, M., Angeli, L., & Papale, D. (2013). Simulation of grassland productivity by the combination of ground and satellite data. *Agriculture, Ecosystems and Environment*, *165*, 163–172.
- Maselli, F., Chiesi, M., Brillì, L., & Moriondo, M. (2012). Simulation of olive fruit yield in Tuscany through the integration of remote sensing and ground data. *Ecological Modelling*, *244*, 1–12. <https://doi.org/10.1016/j.ecolmodel.2012.06.028>
- Maselli, F., Gilabert, M. A., & Conese, C. (1998). Integration of high and low resolution NDVI data for monitoring vegetation in Mediterranean environments. *Remote Sensing of Environment*, *63*(3), 208–218. [https://doi.org/10.1016/S0034-4257\(97\)00131-4](https://doi.org/10.1016/S0034-4257(97)00131-4)
- Matese, A., & Di Gennaro, S. F. (2021). Beyond the traditional NDVI index as a key factor to mainstream the use of UAV in precision viticulture. *Scientific Reports*, *11*(1), 1–13.
- Matese, A., Toscano, P., Di Gennaro, S. F., Genesio, L., Vaccari, F. P., Primicerio, J., Belli, C., Zaldei, A., Bianconi, R., & Gioli, B. (2015). Intercomparison of UAV, aircraft and satellite remote sensing platforms for precision viticulture. *Remote Sensing*, *7*(3), 2971–2990.
- Mezghani, M. A., Hassouna, G., Ibtissem, L., & Labidi, F. (2016). Leaf area index and light distribution in olive tree canopies (*Olea europaea* L.). *International Journal of Agronomy and Agricultural Research*, *8*(5), 60–65. <https://doi.org/10.13140/RG.2.1.3193.5600>
- Moriondo, M., Bindi, M., Fagarazzi, C., Ferrise, R., & Trombi, G. (2011). Framework for high-resolution climate change impact assessment on grapevines at a regional scale. *Regional Environmental Change*, *11*(3), 553–567. <https://doi.org/10.1007/s10113-010-0171-z>
- Moriondo, M., Jones, G. V., Bois, B., Dibari, C., Ferrise, R., Trombi, G., & Bindi, M. (2013). Projected shifts of wine regions in response to climate change. *Climatic Change*, *119*(3–4), 825–839. <https://doi.org/10.1007/s10584-013-0739-y>
- Moriondo, M., Leolini, L., Brillì, L., Dibari, C., Tognetti, R., Giovannelli, A., Rapi, B., Battista, G., Caruso, G., Gucci, R., Argenti, G., Raschi, A., Centritto, M., Cantini, C., & Bindi, M. (2019). A simple model simulating development and growth of an olive grove. *European Journal of Agronomy*, *105*, 129–145.

- Moriondo, M., Maselli, F., & Bindi, M. (2007). A simple model of regional wheat yield based on NDVI data. *European Journal of Agronomy*, 26(3), 266–274. <https://doi.org/10.1016/j.eja.2006.10.007>
- Moulin, S., Bondeau, A., & Delecalle, R. (1998). Combining agricultural crop models and satellite observations: From field to regional scales. *International Journal of Remote Sensing*, 19(6), 1021–1036.
- Munitz, S., Schwartz, A., & Netzer, Y. (2020). Effect of timing of irrigation initiation on vegetative growth, physiology and yield parameters in Cabernet Sauvignon grapevines. *Australian Journal of Grape and Wine Research*, 26(3), 220–232.
- Myneni, R. B., & Williams, D. L. (1994). On the relationship between FAPAR and NDVI. *Remote Sensing of Environment*, 49, 200–211.
- Naor, A., Gal, Y., & Bravdo, B. (2002). Shoot and cluster thinning influence vegetative growth, fruit yield, and wine quality of Sauvignon blanc' grapevines. *Journal of the American Society for Horticultural Science*, 127(4), 628–634.
- Nendel, C., & Kersebaum, K. C. (2004). A simple model approach to simulate nitrogen dynamics in vineyard soils. *Ecological Modelling*, 177(1–2), 1–15.
- OIV. (2020). *State of the world vitiviniculural sector in 2020*. Retrieved from <https://www.oiv.int/public-medias/7909/oiv-state-of-the-world-vitiviniculural-sector-in-2020.pdf>. Accessed 2 May 2021.
- Orlandini, S., Marta, A. D., & Mattii, G. B. (2008). Analysis and agrometeorological modelling of grapevine responses to different trellising system. *Vitis*, 47(2), 89.
- Palliotti, A., Silvestroni, O., & Petoumenou, D. (2009). Photosynthetic and photoinhibition behavior of two field-grown grapevine cultivars under multiple summer stresses. *American Journal of Enology and Viticulture*, 60(2), 189–198.
- Panigrahy, S., Mukherjee, J., Chaudhari, K. N., Parihar, J. S., Ray, S. S., Patel, N. K., & Tripathy, R. (2012). Forecasting wheat yield in Punjab state of India by combining crop simulation model WOFOST and remotely sensed inputs. *Remote Sensing Letters*, 4, 19–28.
- Picón-Toro, J., González-Dugo, V., Uriarte, D., Mancha, L. A., & Testi, L. (2012). Effects of canopy size and water stress over the crop coefficient of a “Tempranillo” vineyard in south-western Spain. *Irrigation Science*, 30(5), 419–432. <https://doi.org/10.1007/s00271-012-0351-3>
- Pinty, B., & Verstraete, M. M. (1992). GEMI: A non-linear index to monitor global vegetation from satellites. *Vegetatio*, 101(1), 15–20.
- Ritchie, J. T., & Otter, S. (1985). *Description and performance of CERES-Wheat: A user-oriented wheat yield model* (Vol. 38, pp. 159–175). United States Department of Agriculture, Agricultural Research Services.
- Rondeaux, G., Steven, M., & Baret, F. (1996). Optimization of soil-adjusted vegetation indices. *Remote Sensing of Environment*, 55(2), 95–107.
- Rouse, J. W., Haas, R. H., Schell, J. A., & Deering, D. W. (1974). Monitoring vegetation systems in the Great Plains with ERTS. *NASA Special Publication*, 351, 309.
- Santos, J. A., Fraga, H., Malheiro, A. C., Moutinho-Pereira, J., Dinis, L. T., Correia, C., Moriondo, M., Leolini, L., Dibari, C., Costafreda-Aumedes, S., Kartschall, T., Menz, C., Molitor, D., Junk, J., Beyer, M., & Schultz, H. R. (2020). A review of the potential climate change impacts and adaptation options for European viticulture. *Applied Sciences (switzerland)*, 10(9), 1–28. <https://doi.org/10.3390/app10093092>
- Setiyono, T. D., Quicho, E. D., Gatti, L., Campos-Taberner, M., Busetto, L., Collivignarelli, F., Garcia-Haro, F. J., Boschetti, M., Khan, N. I., & Holecz, F. (2018). Spatial rice yield estimation based on MODIS and Sentinel-1 SAR data and ORYZA crop growth model. *Remote Sensing*, 10(2), 1–20. <https://doi.org/10.3390/rs10020293>
- Sinclair, T. R. (1986). Water and nitrogen limitations in soybean grain production I. Model development. *Field Crops Research*, 15(2), 125–141. [https://doi.org/10.1016/0378-4290\(86\)90082-1](https://doi.org/10.1016/0378-4290(86)90082-1)
- Soltani, A., & Sinclair, T. R. (2012). *Modeling physiology of crop development, growth and yield*. CABi.
- Sozzi, M., Kayad, A., Marinello, F., Taylor, J., & Tisseyre, B. (2020). Comparing vineyard imagery acquired from Sentinel-2 and Unmanned Aerial Vehicle (UAV) platform. *OENO One*, 54(2), 189–197.
- Stöckle, C. O., Donatelli, M., & Nelson, R. (2003). CropSyst, a cropping systems simulation model. *European Journal of Agronomy*, 18(3–4), 289–307.
- Sun, L., Gao, F., Anderson, M. C., Kustas, W. P., Alsina, M. M., Sanchez, L., Sams, B., McKee, L., Dulaney, W., White, W., Alfieri, J., Prueger, J. H., Melton, F., & Post, K. (2017). Daily mapping of 30 m LAI and NDVI for grape yield prediction in California vineyards. *Remote Sensing*, 9(4), 317.
- Van Leuken, H., & Seligman, N. G. (1987). Simulation of water use, nitrogen nutrition and growth of a spring wheat crop. In H. Van Leuken & N. G. Seligman (Eds.), *Simulation monographs*. Pudoc.

- Vivin, P. H., Castelan, M., & Gaudillère, J. P. (2002). A source/sink model to simulate seasonal allocation of carbon in grapevine. VI International Symposium on computer modelling in fruit research and Orchard management. *Acta Horticulturae*, 584, 43–56.
- Wang, L., Tian, Y., Yao, X., Zhu, Y., & Cao, W. (2014). Predicting grain yield and protein content in wheat by fusing multi-sensor and multi-temporal remote-sensing images. *Field Crops Research*, 164, 178–188.
- Welles, J. M., & Norman, J. M. (1991). Instrument for indirect measurement of canopy architecture. *Agronomy Journal*, 83(5), 818–825.
- Wermelinger, B., Baumgärtner, J., & Gutierrez, A. P. (1991). A demographic model of assimilation and allocation of carbon and nitrogen in grapevines. *Ecological Modelling*, 53, 1–26.
- Wolkovich, E. M., García de Cortázar-Atauri, I., Morales-Castilla, I., Nicholas, K. A., & Lacombe, T. (2018). From Pinot to Xinomavro in the world's future wine-growing regions. *Nature Climate Change*, 8(1), 29–37. <https://doi.org/10.1038/s41558-017-0016-6>
- Zhao, Y., Chen, S., & Shen, S. (2013). Assimilating remote sensing information with crop model using Ensemble Kalman Filter for improving LAI monitoring and yield estimation. *Ecological Modelling*, 270, 30–42.
- Zhou, X., Zheng, H. B., Xu, X. Q., He, J. Y., Ge, X. K., Yao, X., Cheng, T., Zhu, Y., Cao, W. X., & Tian, Y. C. (2017). Predicting grain yield in rice using multi-temporal vegetation indices from UAV-based multi-spectral and digital imagery. *Journal of Photogrammetry and Remote Sensing*, 130, 246–255.
- Ziliani, M. G., Parkes, S. D., Hoteit, I., & McCabe, M. F. (2018). Intra-season crop height variability at commercial farm scales using a fixed-wing UAV. *Remote Sensing*, 10(12), 2007.

Publisher's Note Springer Nature remains neutral with regard to jurisdictional claims in published maps and institutional affiliations.

Authors and Affiliations

L. Leolini¹  · S. Bregaglio²  · F. Ginaldi²  · S. Costafreda-Aumedes^{1,3}  · S. F. Di Gennaro³  · A. Matese³  · F. Maselli³  · G. Caruso⁴  · G. Palai⁴  · S. Bajocco²  · M. Bindi¹  · M. Moriondo^{1,3} 

¹ Department of Agriculture, Food, Environment and Forestry (DAGRI), University of Florence, Piazzale delle Cascine 18, 50144 Florence, Italy

² Research Centre for Agriculture and Environment, CREA - Council for Agricultural Research and Economics, Rome, Italy

³ Institute of BioEconomy (CNR-IBE), National Research Council of Italy, Via Madonna del Piano 10, 50019 Sesto Fiorentino, Italy

⁴ Department of Agriculture, Food and Environment, University of Pisa, Via del Borghetto 80, 56124 Pisa, Italy